

## Article

# Removal of Levofloxacin by Activation of Peroxomonosulfate Using T-POMs@ZIF-67

Yihao Zhang, Ning Kang, Shipu Jiao, Yang Li, Xu Zhang and Xianhua Liu \* 

School of Environmental Science and Engineering, Tianjin University, Tianjin 300354, China; zhangyihao\_@tju.edu.cn (Y.Z.); 2120214001@tju.edu.cn (N.K.); jsp@tju.edu.cn (S.J.); liyang\_@tju.edu.cn (Y.L.); zhangxu\_2022@tju.edu.cn (X.Z.)

\* Correspondence: lxh@tju.edu.cn

**Abstract:** The pyrolysis of metal-organic frameworks (MOFs) is a popular strategy for the synthesis of nanoporous structures. Polymetallic oxides (POMs) are a class of polyhedral structural compounds with unique physicochemical properties. Little effort has been paid to evaluate MOF-POM hybrid-derived materials for peroxomonosulfate (PMS) activation. In this study, a cobalt-based MOF, ZIF-67, together with three types of POMs (phosphomolybdic acid, silicotungstic acid, and phosphotungstic acid), were used as precursors for the synthesis of PMS activation catalyst via pyrolysis. Three T-POMs@ZIF-67 nanohybrids (T-PMo@ZIF-67, T-SiW@ZIF-67, and T-PW@ZIF-67) were obtained by pyrolyzing the prepared precursors at 500 °C. Furthermore, the prepared T-POMs@ZIF-67 nanomaterials were evaluated for the catalytic activation of PMS in the degradation of levofloxacin (LEV). The results showed that the LEV degradation rate could reach 91.46% within 30 min under the optimized conditions when T-PW@ZIF-67 was used as the PMS activation catalyst. The catalytic efficiency of the catalyst decreased by only 9.63% after five cycles, indicating that the material has good stability. This work demonstrates the great potential of POMs@MOF derivatives for application in the field of wastewater treatment.

**Keywords:** MOF derivatives; PMS activation; degradation; organic pollutants



**Citation:** Zhang, Y.; Kang, N.; Jiao, S.; Li, Y.; Zhang, X.; Liu, X. Removal of Levofloxacin by Activation of Peroxomonosulfate Using T-POMs@ZIF-67. *J. Compos. Sci.* **2024**, *8*, 13. <https://doi.org/10.3390/jcs8010013>

Academic Editor: Francesco Tornabene

Received: 22 October 2023

Revised: 25 November 2023

Accepted: 28 December 2023

Published: 29 December 2023



**Copyright:** © 2023 by the authors. Licensee MDPI, Basel, Switzerland. This article is an open access article distributed under the terms and conditions of the Creative Commons Attribution (CC BY) license (<https://creativecommons.org/licenses/by/4.0/>).

## 1. Introduction

Water is the basis for people's survival and is an irreplaceable resource and environmental element [1]. Water resources are precious on Earth; however, water pollution is increasing globally. Organic pollutants, as typical pollutants in water bodies, can come from a variety of sources, such as industrial wastewater, agricultural activities, municipal discharges, chemical use, and domestic wastewater [2–4]. It produces large quantities, has low natural degradation efficiency, and has serious ecological hazards, making it a difficult point in the degradation of pollutants in water bodies [5,6]. An example is levofloxacin (LEV), which is an antibiotic drug widely used to eradicate bacterial diseases [7]. Overuse of LEV increases the amount of LEV-containing wastewater discharged by pharmaceutical companies and hospitals, leading to the formation of drug-resistant genes and increasing the risk of endocrine disruption or cancer [8]. Sulfate radical-based advanced oxidation processes (SR-AOPs) are rapidly developing due to their high oxidation potentials and high selectivity, which have received much attention. Among the catalytic materials capable of activating persulfate to generate  $SO_4^{\cdot -}$ , Metal-organic frameworks (MOFs) derivatives are, moreover, the most promising multiphase catalytic materials for SR-AOPs catalysts.

MOFs have become a popular class of functional materials and precursors for inorganic materials, which have been widely used for electrochemical energy storage and conversion and catalytic degradation of pollutants [9,10]. Among them, MOF derivatives have been applied in the field of catalysis due to their unique nanostructures and good activities. Researchers have successfully synthesized a series of MOF derivatives, such as

transition metal oxides/carbon materials [11–13], transition metal sulfides/carbon materials, transition metal oxides/transition metal oxides [14–17], and other composites [18–20]. Co-MOFs are used as pyrolysis precursors for the preparation of nanostructured functional materials, and metal sulfide/carbon composites can be obtained effortlessly under controlled carbonization conditions. For example, cobalt sulfides are  $\text{Co}_9\text{S}_8$ ,  $\text{CoS}_2$ , and  $\text{Co}_3\text{S}_4$ . Polymetallic oxides (POMs) are a class of polyhedral structural compounds consisting of pre-transition metal atoms bridged by oxygen coordination with specific and superior stereo-structural and physicochemical properties. Multiple electrons and protons can be stored in POM molecules that exhibit reversible redox reaction properties and acid-base properties [21]. In addition, POMs are rich in surface oxygen, so they have high reactivity, which makes them stand out in photocatalytic applications [22].

Composites of POM and MOF show excellent performance in the field of catalysis. POM has good catalytic activity, while MOF can provide highly ordered pore structure and tunable surface properties. Combining them together enables high efficiency and selectivity in catalytic reactions. Sun et al. [23] prepared a composite ( $\text{PW}_{12}@$ Cu-MOF) by encapsulating Keggin-type  $[\text{PW}_{12}\text{O}_{40}]^{3-}$  ( $\text{PW}_{12}$ ) in a copper violet fine framework,  $\text{Cu}_2(\text{CPBPY})_4(\text{H}_2\text{O})_2$  (Cu-MOF). The degradation of methylene blue (MB: 10 mg/L, pH 6.3) by  $\text{PW}_{12}@$ Cu-MOF (0.05 g) was studied under light irradiation at various wavelengths. It was found that the electron-hole pairs in the composites could be excited by both near-infrared (NIR) and visible light radiation, and about 98.2% of MB was degraded within 60 min under visible light irradiation, and about 97.7% of MB was degraded within 100 min under NIR irradiation. Zhao et al. [24] synthesized two stabilized three-dimensional polymetallic oxalate metal-organic skeletons based on Keggin-type POMs, namely,  $[\text{Cu}_{12}(\text{trz})_8(\text{H}_2\text{O})_2][\alpha\text{-SiW}_{12}\text{O}_{40}] \cdot 2\text{H}_2\text{O}$  and  $[\text{Cu}_{12}(\text{trz})_8\text{Cl}][\alpha\text{-PW}_{12}\text{O}_{40}]$ . 40 mg of the two prepared materials were added into 100 mL of  $1.0 \times 10^{-5}$  mol/L Rhodamine B (RhB) aqueous solution. After 240 min of visible light irradiation with a 300 W Xe lamp, the degradation rates of RhB were 91% and 81%, respectively. Recently, Wang et al. [25] prepared ZIF-67@ $\text{SiO}_2$  by adding tetraethyl orthosilicate during the synthesis of ZIF-67, and Co@Si nanocages were prepared by sulfating ZIF-67@ $\text{SiO}_2$  with thioacetamide. It was able to activate PMS to completely remove sulfamethoxazole within 10 min and showed good catalytic performance. In addition, Yang et al. [26] report the design and preparation of hierarchical hollow Mo/Co bimetallic oxide nanocages (Mo/Co HHBONs) derived from polyoxometalate-coupled metal-organic framework (POM@MOF) hybrids for peroxomonosulfate (PMS) activated degradation of levofloxacin.

ZIF-67, as a cobalt-based MOF, has the advantages of high porosity and large cavity structure. Loading the polymetallic oxygenate ions into the cavities of ZIF-67 is the best choice for the preparation of Co-Mo/Co-W oxides characterized by the desired hollow porous structure. Studies on the degradation of pollutants by Co-Mo oxides have been reported. However, there are very few studies on the degradation of pollutants by different types of POM doped with ZIF-67, especially Co-W bimetallic oxides. Therefore, in this paper, different PMOs (phosphomolybdic acid, silicotungstic acid, and phosphotungstic acid) were doped during the preparation of ZIF-67 to obtain POMs@ZIF-67 materials, and T-POMs@ZIF-67 catalysts were prepared after calcination. Its performance in catalyzing the activation of peroxomonosulfate (PMS) for the degradation of levofloxacin (LEV) in an aqueous environment was explored for the first time. See Figure 1 for a schematic diagram.

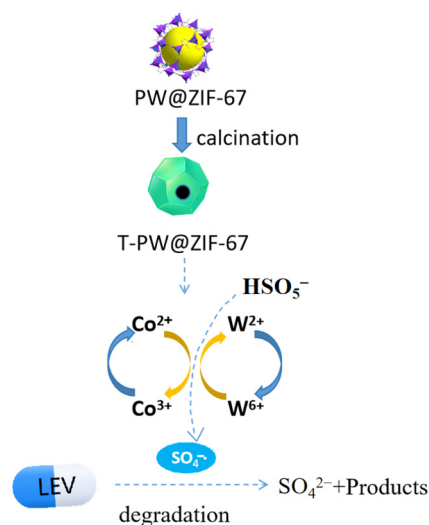


**Figure 1.** Schematic diagram of levofloxacin removal by activation of peroxomonosulfate using T-PW@ZIF-67.

## 2. Materials and Methods

### 2.1. Characterization

SEM image using scanning electron microscope (S4800, Hitachi High-tech Corporation, Tokyo, Japan). XRD analysis by X-ray diffractometer (D/MX-III A, Hitachi High-tech Corporation, Japan). XPS analysis using X-ray photoelectron spectrometer (Escalab 250Xi, Thermo Fisher Scientific, Waltham, MA, USA).

### 2.2. Preparation of Catalysts

#### 2.2.1. Preparation of POMs@ZIF-67

POMs@ZIF-67 was synthesized from a previous report [27] with some modifications. 2.5 mM Co(NO<sub>3</sub>)<sub>2</sub>·6H<sub>2</sub>O was dissolved in 25 mL of methanol solution and later mixed with 10 mL of POMs aqueous solution (30 mM), noted as solution A. In this work, three heteropoly acids were used to prepare POMs@ZIF-67, which were phosphomolybdic acid (H<sub>3</sub>[P(Mo<sub>3</sub>O<sub>10</sub>)<sub>4</sub>], PMo<sub>12</sub>), silicotungstic acid (H<sub>3</sub>[Si(W<sub>3</sub>O<sub>10</sub>)<sub>4</sub>], SiW<sub>12</sub>) and phosphotungstic acid (H<sub>3</sub>[P(W<sub>3</sub>O<sub>10</sub>)<sub>4</sub>], PW<sub>12</sub>). 20 mM 2-methylimidazole was added to 25 mL of methanol solution, noted as solution B. Solution B was quickly added to solution A and mixed well to obtain solution C. The solution C was moved to a hydrothermal reactor and heated at 120 °C for 10 h to obtain a purple precipitate. It was filtered and washed with ethanol, after which it was dried overnight at 60 °C to finally obtain POMs@ZIF-67 materials (PMo@ZIF-67, SiW@ZIF-67, PW@ZIF-67).

#### 2.2.2. Preparation of T-POMs@ZIF-67

The prepared POMs@ZIF-67 were placed in a muffle furnace and slowly heated to 500 degrees for 2 h. The materials were washed with ethanol after cooling down and dried overnight at 60 °C to obtain POMs@ZIF-67 oxides (T-PMo@ZIF-67, T-SiW@ZIF-67, T-PW@ZIF-67).

#### 2.2.3. Synthesis of CoWO<sub>4</sub> Nanomaterials

CoWO<sub>4</sub> was synthesized from a previous report [28], with some modifications. Dissolve Co(NO<sub>3</sub>)<sub>2</sub>·6H<sub>2</sub>O and NaWO<sub>4</sub> (Co/Mo molar mass ratio = 1:1) in deionized water and stir vigorously for 30 min. The mixture was transferred to a hydrothermal reactor, heated to 120 °C, and kept for 10 h. The resulting powder was washed six times using a mixture of deionized water and ethanol (1:1, v/v) after cooling. Finally, the solid was dried at 70 °C overnight and later calcined at 500 °C for 2 h to obtain CoWO<sub>4</sub> nanomaterials.

### 2.3. Experimental Methods

#### 2.3.1. LEV Degradation Test

The standard curve of LEV was plotted based on the relationship between concentration and absorbance. LEV solutions of 0.25, 5, 10, 15, 20, 25, and 30 mg/L were prepared, and the absorbance of the LEV solutions was determined on a UV-visible spectrophotometer (Mapada, Shanghai, China) at the maximum absorption wavelength of 287 nm. A typical reaction was conducted in a 250-mL glass beaker reactor with a 100 mL reaction solution containing 1 mg LEV, 0.035 mM potassium persulfate, and 5 mg of catalyst. 2.5 mL samples were withdrawn every 3 min by a syringe and injected into a vial through a 0.22  $\mu\text{m}$  filtration membrane. The results were tested by UV spectrophotometer, and each degradation experiment was performed three times. The LEV degradation was calculated as below.

$$\text{LEV degradation (\%)} = \frac{C_0 - C_t}{C_0} \times 100\% \quad (1)$$

where  $C_0$  is the initial concentration of the LEV and  $C_t$  is the LEV concentration at moment  $t$ .

#### 2.3.2. Recyclability Test

In the recycling tests, the catalysts were separated by filtration after every cycle experiment, washed with a mixed ethanol-water solution, and dried at 50  $^{\circ}\text{C}$  for the subsequent reaction.

## 3. Results and Discussion

### 3.1. Characterization of T-PW@ZIF-67

#### 3.1.1. X-ray Diffraction Analysis

X-ray Diffraction (XRD) characterization of T-ZIF-67 and T-PW@ZIF-67 was carried out, and the results obtained are shown in Figure 2a. The comparison reveals that the catalyst only exhibits an enhancement of the peak intensity, suggesting that this polyhedron is still predominantly a ZIF-67-like structure. However, compared with the narrow and sharp diffraction peaks of  $\text{Co}_3\text{O}_4$  produced by pristine ZIF-67 calcination, the peak widths of  $\text{Co}_3\text{O}_4$  in all  $\text{Co}_3\text{O}_4/\text{CoWO}_4$  samples become wider and larger, indicating a significant decrease in grain size. The XRD results showed that the calcined PW@ZIF-67 catalysts  $\text{Co}_3\text{O}_4$  and  $\text{CoWO}_4$  coexist. Diffraction peaks at  $2\theta$  of 19.2 $^{\circ}$ , 31.7 $^{\circ}$ , 36.8 $^{\circ}$ , and 44.6 $^{\circ}$  are associated with peaks of (111), (220), (311), and (400)  $\text{Co}_3\text{O}_4$  (JCPDS No. 42-1467). The presence of diffraction peaks with  $2\theta$  of 24.0 $^{\circ}$ , 24.7 $^{\circ}$ , 34.8 $^{\circ}$ , and 44.5 $^{\circ}$  labeled the presence of  $\text{CoWO}_4$  (JCPDS No. 82-2339). Up to this point, the XRD results demonstrated that the  $\text{Co}_3\text{O}_4/\text{CoWO}_4$  hybrids were successfully obtained by one-step calcination of PW@ZIF-67.

#### 3.1.2. Scanning Electron Microscope Analysis

Figure 2b shows the microstructure of T-PW@ZIF-67. The calcined PW@ZIF-67 morphology is ortho-dodecahedral, and the diameter of T-PW@ZIF-67 particles is about 500 nm. Its rough surface increases the number of active sites involved in the activation of PMS for LEV degradation [26]. After calcination, the elements carbon, cobalt, tungsten, oxygen, and phosphorus are uniformly distributed throughout the structure. It can be proved that  $\text{H}_3[\text{P}(\text{W}_3\text{O}_{10})]_4$  is uniformly distributed into the pores of ZIF-67 without obvious agglomeration during the preparation process, and the elements are uniformly distributed in the samples after calcination and pyrolysis. This unique hollow structure of T-PW@ZIF-67 is likely to be associated with an inside-out Ostwald ripening mechanism due to the coordinated action of  $\text{H}_3[\text{P}(\text{W}_3\text{O}_{10})]_4$  and anisotropic corrosion during hybrid self-assembly. In addition, the energy dispersive spectra (EDS) of the calcined cobalt-tungsten oxides were characterized (Figure 2c). In this catalyst, the molar mass ratio of Co to W is 2.68:1, from which the molar mass ratio of  $\text{Co}_3\text{O}_4$  to  $\text{CoWO}_4$  can be calculated to be 0.56:1.

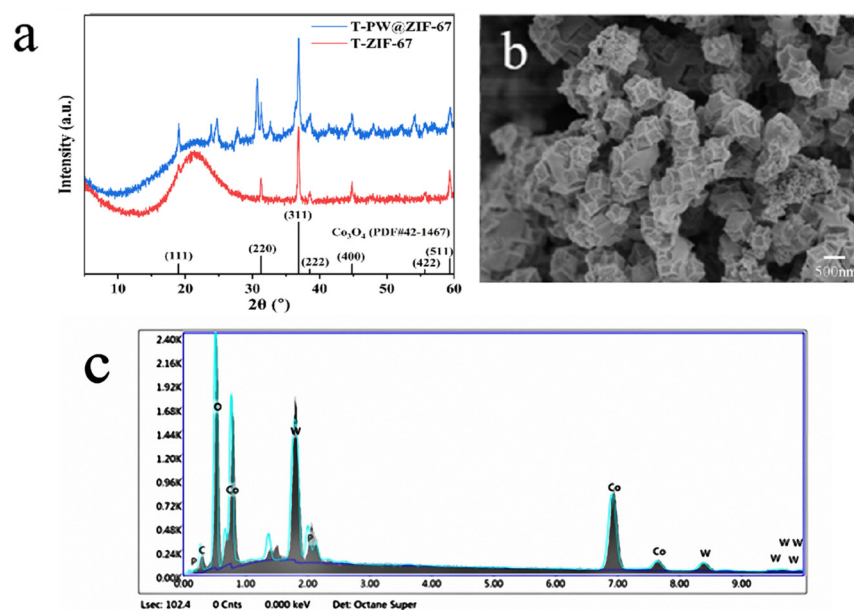


**Figure 2.** (a) XRD image of T-PW@ZIF-67; (b) SEM image of T-PW@ZIF-67; (c) EDS plot of T-PW@ZIF-67.

### 3.1.3. X-ray Photoelectron Spectroscopy Analysis

Figure 3a shows the XPS spectra of the individual elements of the whole catalyst with peaks at 780.76 eV, 530.76 eV, 284.03 eV, and 36.18 eV for Co2p, O1s, C1s, and W4f. The peaks centered at 284.77 eV, 286.38 eV, and 288.63 eV shown in Figure 3b represent C=C/C-C, C=C/C-C, and C=O for the signals of C1s. In Figure 3c, the three peaks at 530.17 eV, 530.94 eV, and 530.06 eV binding energies then represent lattice oxygen, oxygen vacancies, and adsorbed oxygen, respectively (Figure 3c). By comparison with the XPS plot of the T-ZIF67 catalyst, it was found that the lattice oxygen peak was positively shifted by 0.1 eV upon the addition of phosphomolybdic acid. The XPS pattern of W4f is shown in Figure 3d with two splits at 35.31 eV and 37.45 eV and a column width of 2.14 eV, similar to that in the literature, which can be determined to be  $W^{6+}$ . The spectrum of Co2p (Figure 3e) shows two spin-orbit double peaks with an orbital splitting width of 15 eV and multiple signal peaks. The spin-orbit double peaks at positions 780 eV and 795 eV in the figure represent the Co2p<sub>3/2</sub> and Co2p<sub>1/2</sub> energy levels of the Co ion, respectively. The main peaks, which can be divided into three pairs of double peaks, and the signal peaks at high binding energies at distances of 6 eV and 8 eV from the main peaks, all indicate the presence of both Co<sup>2+</sup> and Co<sup>3+</sup> in the material. The binding energy potential of the peak of the phosphotungstic acid doped catalyst is positively shifted by 0.16 eV, which indicates that the doping of W ions decreases the electron density of Co ions. It makes Co ions more electrophilic, which increases their surface-active substances and is more helpful in activating PMS to degrade LEV.

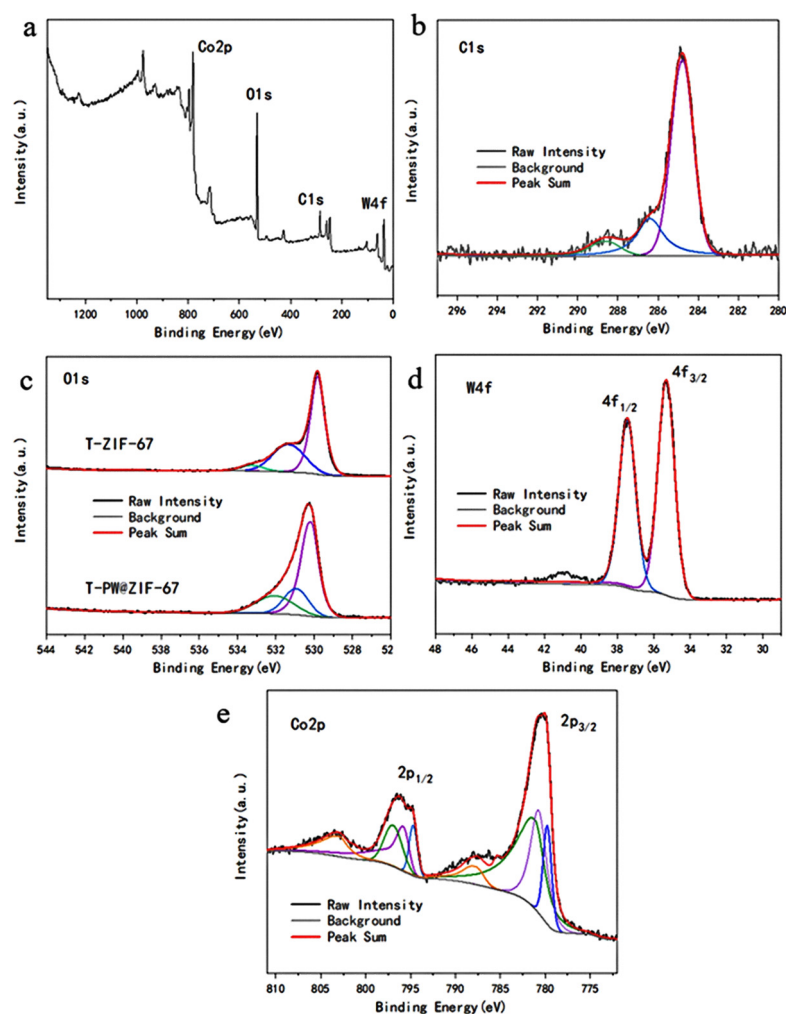


**Figure 3.** (a) Full spectrum of XPS at T-PW@ZIF-67; (b) C1s spectra; (c) O1s spectra; (d) W4f spectra; (e) Co2p spectra.

### 3.2. PMS Activation by T-POMs@ZIF-67 for LEV Degradation

#### 3.2.1. Activity Comparison of Different T-POMs @ZIF-67

The catalytic ability of different T-POMs@ZIF-67 for LEV degradation via PMS activation was investigated (Figure 4a). The catalytic ability for LEV degradation is PMS < T-ZIF67 < CoW < T-SiW@ZIF-67 < T-PMo@ZIF-67 < T-PW@ZIF-67. T-PW@ZIF-67 showed the best performance, and the degradation rate of LEV reached 80.11% within 3 min and reached 91.46% in 30 min. The high performance of T-PW@ZIF-67 may be due to the following: (1) the combination of the Keggin-structured phosphotungstic acid with ZIF-67 can greatly increases its active site; (2) the interaction between  $\text{Co}^{2+}$  and  $\text{W}^{2+}$  accelerates the catalytic process, so it takes less time to activate PMS to degrade LEV. The degradation rate of CoW was much lower than that of the T-PW@ZIF-67, and only 61.32% of LEV was removed at 30 min. It may be due to its surface tension and magnetic property that makes it easy to agglomerate. These results confirm that the combination of ZIF-67 with POMs can generate more active sites for PMS activation after pyrolysis.

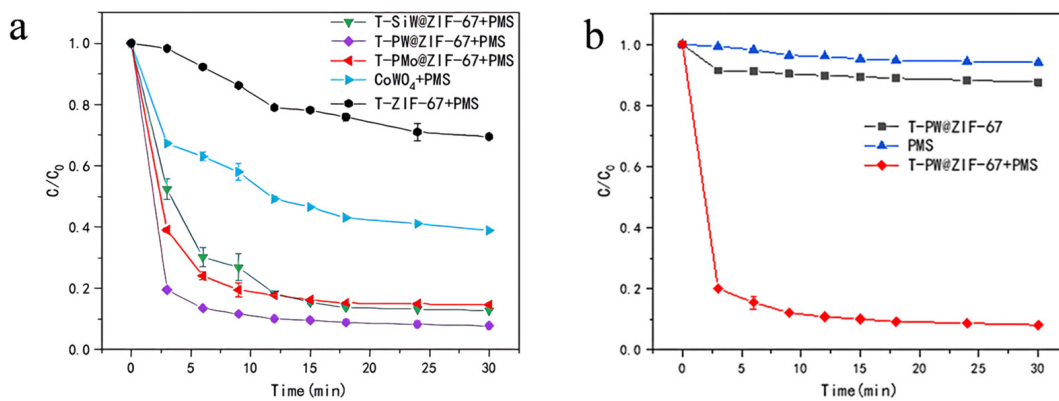


**Figure 4.** (a) Activity of different T-POMs@ZIF-67 for LEV degradation via PMS activation; (b) Effect of PMS on the catalytic efficiency of T-PW@ZIF-67 for LEV degradation.

In order to investigate the performance of the T-PW@ZIF-67 catalyst to activate PMS, the degradation rate of LEV was measured under two different conditions: with PMS without T-PW@ZIF-67 and with T-PW@ZIF-67 without PMS (Figure 4b). It can be seen that the efficiency of PMS itself for LEV degradation is very low, and the degradation rate is only 5% at 30 min. T-PW@ZIF-67 itself also has negligible performance for LEV degradation, and the degradation rate of LEV is only 10% at 30 min. These results demonstrated that the high degradation efficiency of LEV is via the PMS activation by T-PW@ZIF-67.

### 3.2.2. Effect of Doping Amount of Phosphotungstic Acid and Pyrolysis Temperature on the Performance of T-PW@ZIF-67

To further enhance the catalytic performance of T-PW@ZIF-67, different doping amounts of phosphotungstic acid (10 mL of 5, 25, 50, and 75 mM PW, respectively) were added during the synthesis. Catalytic degradation experiments were carried out at room temperature by adding 0.035 mM of potassium persulfate and 5 mg of catalyst to 100 mL of LEV solution with an initial concentration of 10 mg/L at pH = 7.3 (Figure 5a). T-PW@ZIF-67<sub>5</sub> shows the lowest degradation rate, and T-PW@ZIF-67<sub>50</sub> shows the best performance. These results demonstrate that the addition of a moderate amount of phosphotungstic acid promotes the generation of active sites for PMS activation.

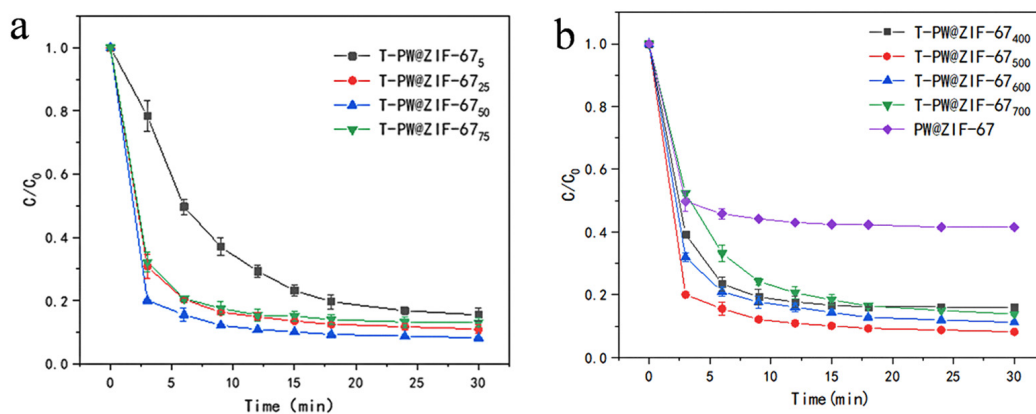


**Figure 5.** (a) Effect of doping amount of phosphotungstic acid on the performance of T-PW@ZIF-67; (b) Effect of pyrolysis temperature on the performance of T-PW@ZIF-67.

In order to investigate the effect of pyrolysis temperature on the performance of T-PW@ZIF-67, PW@ZIF-67 was calcined at 400 °C, 500 °C, 600 °C and 700 °C, respectively. Four T-PW@ZIF-67 materials were obtained for the catalytic experiments, and their performance is shown in Figure 5b. The degradation rates were significantly different at

different calcination temperatures, T-PW@ZIF-67<sub>700</sub> < T-PW@ZIF-67<sub>400</sub> < T-PW@ZIF-67<sub>600</sub> < T-PW@ZIF-67<sub>500</sub>. T-PW@ZIF-67<sub>700</sub> shows the worst performance with a degradation rate of 51.22% at 3 min. PW@ZIF-67<sub>500</sub> shows the best performance with a degradation rate of more than 80% after 3 min. The best catalytic ability of PW@ZIF-67<sub>500</sub> is supposedly due to the fact that the ZIF-67 structure is no longer stable at environments higher than 550 °C and is prone to collapse [29].

### 3.2.3. Effect of PMS Dosage on LEV Degradation Catalyzed by T-PW@ZIF-67

After activation, PMS can provide important reactants (SO<sub>4</sub><sup>-·</sup> and ·OH) involved in the LEV degradation reaction. In order to realize efficient PMS activation for LEV degradation, the effect of persulfate dosage on the catalytic performance of T-PW@ZIF-67 was investigated. During the experiment, 0.01 mM–0.05 mM of potassium persulfate was added respectively. Figure 6 shows the experimental results. The degradation efficiency of LEV gradually increased with the increase of PMS addition, and the reaction gradually stabilized after 10 min. When the dosage was increased from 0.01 mM to 0.035 mM, the removal of LEV increased from 49.58% to 79.89% at 3 min and from 58.91% to 91.59% at 30 min. However, when the dosage was increased from 0.035 mM to 0.05 mM, the LEV removal rate changed insignificantly. The possible reasons for this are as follows: (1) PMS dose was the rate-limiting factor for LEV degradation at low PMS dose. Meanwhile, the active site gradually saturated at high PMS doses, suggesting that the number of T-PW@ZIF-67 active sites is a critical limitation [30]; (2) the radicals can react with the excess PMS in a quenching reaction:

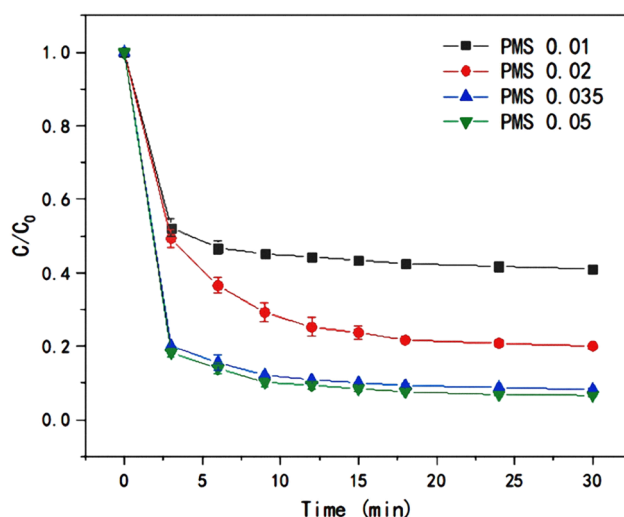
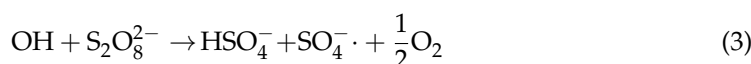
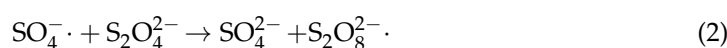
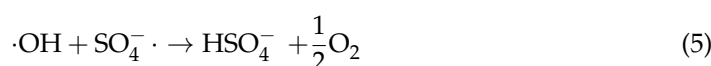


Figure 6. Effect of PMS dosage on the efficiency of LEV degradation catalyzed by T-PW@ZIF-67.

Self-quenching reactions also occur between free radicals due to the increase concentration of radicals:



When PMS concentration is too high, the rapid depletion of PMS and free radicals results in no significant change in the concentration of active substances. Thus, the removal rate of LEV was not significantly increased. Therefore, the optimal dosage of PMS was 0.35 mM.

### 3.2.4. Effect of Initial LEV Concentration on the Performance of T-PW@ZIF-67

The initial concentration of LEV has an important effect on the efficiency of T-PW@ZIF-67 in activating PMS. Three different initial concentrations of LEV were selected: 5 mg/L, 10 mg/L, and 15 mg/L. As shown in Figure 7, the degradation rate gradually decreased as the initial concentration of LEV increased, and the time for the reaction to reach equilibrium was also gradually extended. T-PW@ZIF-67 needs PMS to produce a quantitative amount of active substances. When the concentration of LEV increased, it resulted in insufficient quantitative active substances to react with LEV, which led to a significant decrease in the degradation rate.

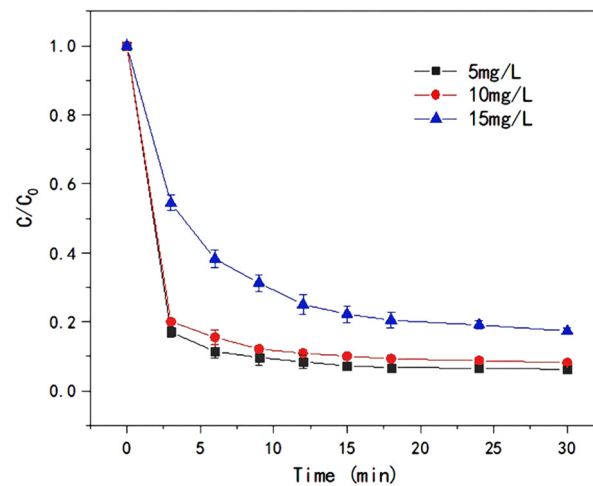


**Figure 7.** Effect of LEV concentrations on the efficiency of LEV degradation by T-PW@ZIF-67.

### 3.2.5. Effect of pH on the Catalytic Performance of T-PW@ZIF-67

The effect of pH in the range of 2.0 to 9.0 on the catalytic performance of T-PW@ZIF-67 is shown in Figure 8. The lowest removal rate of LEV was observed when the pH was 3.0, which was only 20.06% at 3 min, and the reaction gradually stabilized at 18 min. At pH 5.0, the removal rate was 60% at 3 min and 90.01% at 30 min. Under strongly acidic conditions,  $H^+$  can react with  $\cdot OH$  to produce  $H_2O$ . In this way, free radicals are consumed, leading to a decrease in the degradation rate of LEV [26]. When the pH value was 9.0, the removal of LEV was only 57.24% at 3 min, which showed that the alkaline environment is also unfavorable for the activation of PMS by T-PW@ZIF-67. The reason may be that  $OH^-$  can react with  $SO_4^{\cdot -}$ , and the active substances involved in the reaction are reduced.

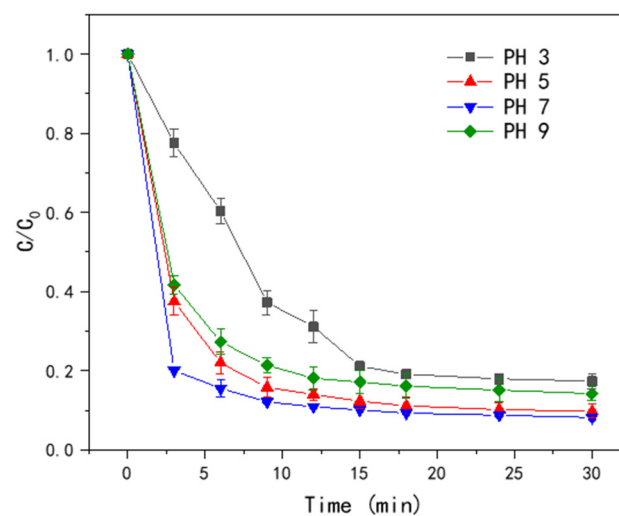


**Figure 8.** Effect of different PH on the efficiency of LEV degradation by T-PW@ZIF-67.

### 3.2.6. Effect of Co-Existing Ions on the Catalytic Performance of T-PW@ZIF-67

In practice, organic wastewater often contains many anions and organics. Common anions in water are  $\text{Cl}^-$ ,  $\text{HCO}_3^-$ , and  $\text{H}_2\text{PO}_4^-$ , all of which may affect the effectiveness of catalyst activation of PMS for LEV degradation. In order to investigate the activated degradation effect of the catalyst in different anionic environments, the reaction system was placed in the environment of  $\text{Cl}^-$ ,  $\text{HCO}_3^-$ , and  $\text{H}_2\text{PO}_4^-$  at concentrations of 0.3, 3, and 30 mM/L, respectively, and the experimental results are shown in Figure 9.

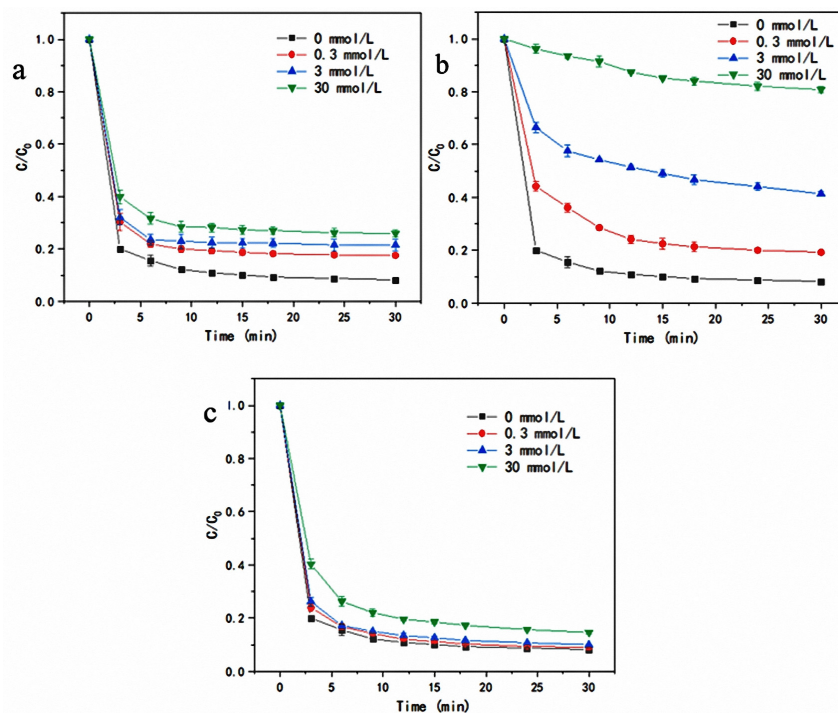


**Figure 9.** (a) Effect of  $\text{Cl}^-$  concentration on LEV degradation efficiency; (b) Effect of  $\text{HCO}_3^-$  concentration on LEV degradation efficiency; (c) Effect of  $\text{H}_2\text{PO}_4^-$  concentration on LEV degradation efficiency.

The results of the effect of  $\text{Cl}^-$  concentration on the activation of T-PW@ZIF-67 to degrade LEV are shown in Figure 9a. As the concentration of  $\text{Cl}^-$  increased, the degradation rate of LEV gradually decreased, and when the concentration was increased from 0 to 30 mM/L, the removal rate decreased from 91.46% to 74.88% at 30 min. However, the time for their reactions to reach equilibrium was not significantly prolonged, and all of them equilibrated after 9 min with no significant change in the degradation rate. The reason for this result may be that  $\text{Cl}^-$  itself is a free radical quencher and reacts with  $\cdot\text{OH}$  and  $\text{SO}_4^{\cdot-}$  in the reaction system of Equations (6) and (7) [31,32]. It leads to the depletion of the reactive substances and, thus, a significant decrease in the degradation rate of LEV.



The results of the effect of  $\text{HCO}_3^-$  concentration on the activity of T-PW@ZIF-67 are shown in Figure 9b. As the concentration of  $\text{HCO}_3^-$  increased from 0 mM to 30 mM, the degradation rate gradually decreased. When the  $\text{HCO}_3^-$  concentration reached 30 mM, the degradation rate was only 19.4% at 30 min, and the time for the reaction to reach stability changed from 6 min to 30 min. The reason for this phenomenon can be explained as follows: on the one hand, the hydrolysis reaction of  $\text{HCO}_3^-$  in Equation (8) leads to the increase of pH value of the water, which makes the water appear weakly alkaline. The catalyst performance under alkaline conditions is weakened; on the other hand, it is possible that  $\text{HCO}_3^-$  may be quenched with  $\cdot\text{OH}$  and  $\text{SO}_4^{\cdot-}$  in the reaction system

(Equations (9) and (10)) [32], resulting in a reduction of active substances participating in the degradation reaction. At the same time, the quenching reaction will produce  $\text{OH}^-$ , which will increase the pH value of the water body again. Thus, it resulted in a decrease in the degradation rate of LEV, and prolonged stabilization time of the reaction.



The results of the effect of  $\text{H}_2\text{PO}_4^-$  concentration on the catalytic ability of T-PW@ZIF-67 are shown in Figure 9c. The increase of  $\text{H}_2\text{PO}_4^-$  concentration did not significantly affect the degradation rate of LEV, which remained above 90% at 30 min when the  $\text{H}_2\text{PO}_4^-$  concentration was 3 mM. Under 30 mM of  $\text{H}_2\text{PO}_4^-$ , the degradation rate of LEV was 86.18% at 30 min, and all the reactions reached equilibrium within 15 min. This phenomenon may be due to the fact that the presence of  $\text{H}_2\text{PO}_4^-$  does not significantly increase the pH of the water.

### 3.2.7. Effect of Natural Organic Matter in Water on the Catalytic Performance of T-PW@ZIF-67

In actual applications, catalysts are often placed in complex aqueous environments where natural organic matter is a prevalent component. To simulate the situation, T-PW@ZIF-67 was put into the reactor with humic acid concentrations of 1, 3, and 5 mg/L. The result shows that the addition of humic acid significantly reduced the efficiency of catalyst activation of PMS for LEV degradation (Figure 10). At 30 min, the degradation rate of LEV was 85.05%, 82.05%, and 75.22%, respectively. One reason for this phenomenon is that humic acids can compete for the active substances participating in the reaction. On the other hand, humic acid contains a large number of electron-rich hydroxyl and carboxyl groups that are subject to attack by electrophilic radicals [32,33]. These groups adsorb to the catalyst surface, resulting in lower yields of  $\cdot\text{OH}$  and  $\text{SO}_4^{\cdot-}$ .

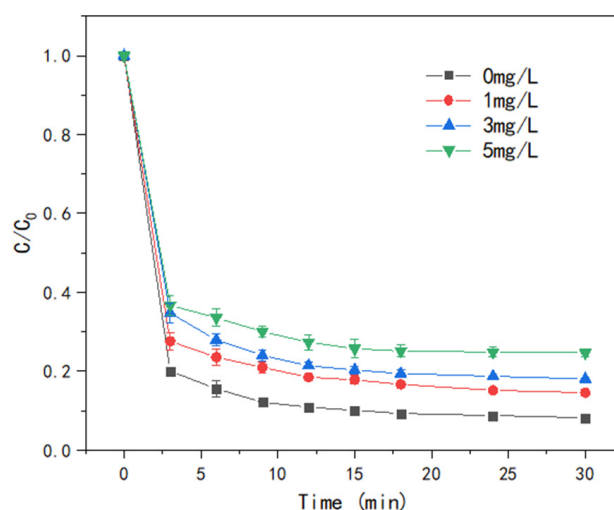


**Figure 10.** Effect of HA concentration on the efficiency of LEV degradation by T-PW@ZIF-67.

### 3.2.8. Stability Analysis of T-PW@ZIF-67

The recyclability of catalysts is an important index for evaluating the goodness of catalysts, which determines the feasibility of their application in practice. The recyclability of the catalysts was evaluated by comparing the degradation rates of five consecutive experiments under the same conditions (Figure 11). The degradation rate of LEV was 92.59% in the first cycle and it was 82.96% in the fifth cycle. The decrease may be related to two factors: (1) Although the amount of  $\text{Co}^{2+}$  increased after the catalytic reaction, it could

not offset the negative effect of W loss. (2) Intermediate byproducts may be adsorbed to the active site, hindering the degradation. The recyclability test demonstrated the material has good stability.

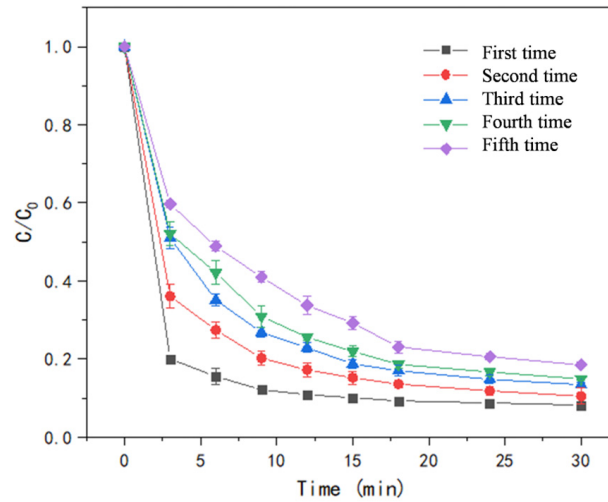
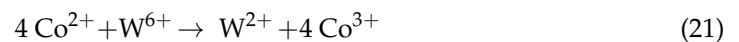
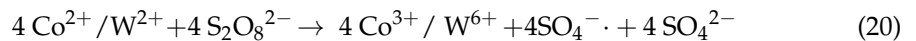
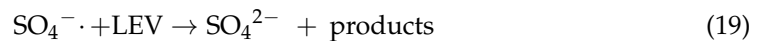
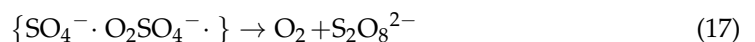
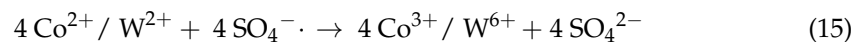
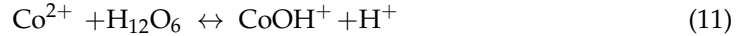


Figure 11. Stability test of T-PW@ZIF-67.

### 3.3. Discussion of Catalytic Mechanism

Combining the results of TEM, XPS, and XRD characterization and activation degradation experiments, the catalytic mechanism can be discussed [29,34,35]. The process of LEV degradation catalyzed by T-PW@ZIF-67 can be summarized as the following reaction:



In the whole reaction process,  $\text{Co}^{2+}$  in the PW@ZIF-67 oxide is first hydrolyzed to form  $\text{CoOH}^+$ , which reacts with PMS to form  $\text{SO}_4^- \cdot$ . The  $\text{CoO}^+$  generated in the process can again continue to react with PMS to generate  $\text{SO}_5^- \cdot$ , at which time  $\text{Co}^{3+} / \text{W}^{6+}$  is reduced to  $\text{Co}^{2+} / \text{W}^{2+}$ , which can again participate in the previous round of reaction.

$\text{Co}^{2+}$  is more effective than  $\text{Co}^{3+}$  in activating PMS because of the higher redox capacity of  $\text{SO}_4^- \cdot$  relative to  $\text{SO}_5^- \cdot$  [33,36]. The oxidizing ability of  $\text{SO}_5^- \cdot$  is weak, so part of it produces  $\text{S}_2\text{O}_8^{2-}$  and part of it produces  $\text{SO}_4^- \cdot$ .  $\text{S}_2\text{O}_8^{2-}$  can return to the reaction as a  $\text{Co}^{2+} / \text{W}^{2+}$  oxidizer, while  $\text{SO}_4^- \cdot$  was produced. There is a synergistic interaction between  $\text{W}^{6+}$  and  $\text{Co}^{2+}$ , on the one hand, it can react with  $\text{Co}^{2+}$  to form  $\text{Co}^{3+}$  with oxidizing properties, on the other hand, it can react with PMS to form  $\text{SO}_5^- \cdot$ .  $\text{SO}_4^- \cdot$  as a free radical can break the chemical chain of LEV and thus be broken down. Moreover,  $\text{SO}_4^- \cdot$  can

further react with water to form  $\cdot\text{OH}$ , which can also participate in the reaction to break the chemical chain of LEV (Figure 12). Intermediates such as decarboxylated levofloxacin, levofloxacin-N-oxide, and demethylated levofloxacin may be produced during degradation. The above intermediates undergo a series of oxidation processes to produce  $\text{CO}_2$  and  $\text{H}_2\text{O}$ .

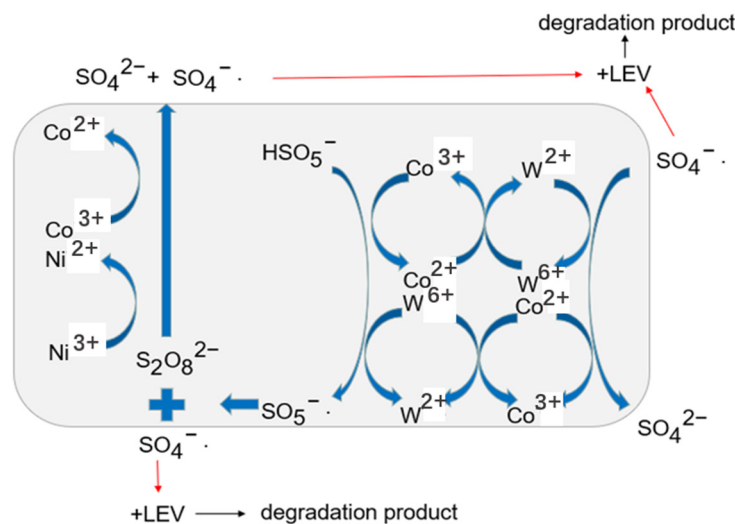


**Figure 12.** Mechanism of LEV degradation by PMS catalyzed with T-PW@ZIF-67.

The stability of the catalyst determines its service life and practical significance.  $\text{Co}^{2+}$  and  $\text{W}^{6+}$  in T-PW@ZIF-67 have a synergistic effect.  $\text{Co}^{3+}$  can be easily obtained by the good oxidizing property of  $\text{W}^{6+}$ , and  $\text{Co}^{3+}$  can be re-reduced to  $\text{Co}^{2+}$  by PMS, thereby realizing the recycling of the catalyst.

#### 4. Conclusions

In this paper, hollow ZIF-67 was utilized to immobilize different POMs to synthesize new catalysts for PMS activation. A series of T-POMs@ZIF-67 catalysts were prepared and evaluated for degradation of LEV via PMS activation. Among the five catalysts (T-PW@ZIF-67, T-SiW@ZIF-67, T-PMo@ZIF-67,  $\text{CoWO}_4$ , and T-ZIF67), T-PW@ZIF-67 showed the highest activity. The degradation rate of LEV reached 80.11% within 3 min under the catalysis of T-PW@ZIF-67. T-PW@ZIF-67 had the best catalytic performance when doped with 30 mM of phosphomolybdic acid solution and being calcined at 500 °C. High PMS concentration, low substrate concentration and neutral pH favor the degradation of LEV. The influence of water quality on the catalyzed degradation was also investigated. With the increase of the concentration of  $\text{Cl}^-$  and  $\text{HCO}_3^-$ , the degradation efficiency tends to decline. The catalysts were sensitive to  $\text{HCO}_3^-$ , but not to  $\text{H}_2\text{PO}_4^-$ . Humic acid, as a reaction competitor, significantly inhibited the degradation efficiency of LEV. T-PW@ZIF-67 kept high recyclability even after 5 cycles. This work indicates that POMs@MOF-derived materials have great potential for wastewater treatment.

**Author Contributions:** Writing—original draft preparation, Y.Z. and N.K.; methodology, S.J.; data curation, Y.L.; conceptualization, X.Z.; writing—review and editing, X.L. All authors have read and agreed to the published version of the manuscript.

**Funding:** This research was funded by the National Key R&D Program of China (Grant No. 2019YFC1407800); the Tianjin Science and Technology Program (Grant No. 21YFSNSN00180); the Tianjin University Postgraduate Arts and Sciences Topnotch Innovation Award Program 2022 Project (No. C1-2022-007).

**Data Availability Statement:** Data are contained within the article.

**Conflicts of Interest:** The authors declare no conflicts of interest.

## References

1. Mekonnen, M.M.; Hoekstra, A.Y. Four billion people facing severe water scarcity. *Sci. Adv.* **2016**, *2*, e1500323. [[CrossRef](#)]
2. Acharya, R.; Lenka, A.; Parida, K. Magnetite modified amino group based polymer nanocomposites towards efficient adsorptive detoxification of aqueous Cr (VI): A review. *J. Mol. Liq.* **2021**, *337*, 116487. [[CrossRef](#)]
3. Mansingh, S.; Acharya, R.; Martha, S.; Parida, K.M. Pyrochlore Ce<sub>2</sub>Zr<sub>2</sub>O<sub>7</sub> decorated over rGO: A photocatalyst that proves to be efficient towards the reduction of 4-nitrophenol and degradation of ciprofloxacin under visible light. *Phys. Chem. Chem. Phys.* **2018**, *20*, 9872–9885. [[CrossRef](#)]
4. Chi, Y.; Yuan, Q.; Li, Y.; Zhao, L.; Li, N.; Li, X.; Yan, W. Magnetically separable Fe<sub>3</sub>O<sub>4</sub>@SiO<sub>2</sub>@TiO<sub>2</sub>-Ag microspheres with well-designed nanostructure and enhanced photocatalytic activity. *J. Hazard. Mater.* **2013**, *262*, 404–411. [[CrossRef](#)]
5. Taghavi, R.; Rostamnia, S.; Farajzadeh, M.; Karimi-Maleh, H.; Wang, J.; Kim, D.; Jang, H.W.; Luque, R.; Varma, R.S.; Shokouhimehr, M. Magnetite metal-organic frameworks: Applications in environmental remediation of heavy metals, organic contaminants, and other pollutants. *Inorg. Chem.* **2022**, *61*, 15747–15783. [[CrossRef](#)]
6. Ma, Z.; Fang, L.; Liu, L.; Hu, B.; Wang, S.; Yu, S.; Wang, X. Efficient decontamination of organic pollutants from wastewater by covalent organic framework-based materials. *Sci. Total Environ.* **2023**, *901*, 166453. [[CrossRef](#)]
7. Mahmoud, M.E.; El-Ghanam, A.M.; Mohamed, R.H.A.; Saad, S.R. Enhanced adsorption of Levofloxacin and Ceftriaxone antibiotics from water by assembled composite of nanotitanium oxide/chitosan/nano-bentonite. *Mater. Sci. Eng. C* **2020**, *108*, 110199. [[CrossRef](#)]
8. Ma, Q.; Zhang, H.; Zhang, X.; Li, B.; Guo, R.; Cheng, Q.; Cheng, X. Synthesis of magnetic CuO/MnFe<sub>2</sub>O<sub>4</sub> nanocomposite and its high activity for degradation of levofloxacin by activation of persulfate. *Chem. Eng. J.* **2019**, *360*, 848–860. [[CrossRef](#)]
9. Jacobs, R.; Patki, P.; Lynch, M.J.; Chen, S.; Morgan, D.; Field, K.G. Materials swelling revealed through automated semantic segmentation of cavities in electron microscopy images. *Sci. Rep.* **2023**, *13*, 5178. [[CrossRef](#)] [[PubMed](#)]
10. Mehtab, T.; Yasin, G.; Arif, M.; Shakeel, M.; Korai, R.M.; Nadeem, M.; Muhammad, N.; Lu, X. Metal-organic frameworks for energy storage devices: Batteries and supercapacitors. *J. Energy Storage* **2019**, *21*, 632–646. [[CrossRef](#)]
11. Han, X.; Chen, W.M.; Han, X.; Tan, Y.Z.; Sun, D. Nitrogen-rich MOF derived porous Co<sub>3</sub>O<sub>4</sub>/N-C composites with superior performance in lithium-ion batteries. *J. Mater. Chem. A* **2016**, *4*, 13040–13045. [[CrossRef](#)]
12. Zhang, H.; Wang, Y.; Zhao, W.; Zou, M.; Chen, Y.; Yang, L.; Xu, L.; Wu, H.; Cao, A. MOF-derived ZnO nanoparticles covered by N-doped carbon layers and hybridized on carbon nanotubes for lithium-ion battery anodes. *ACS Appl. Mater. Inter.* **2017**, *9*, 37813–37822. [[CrossRef](#)] [[PubMed](#)]
13. Wang, Y.; Zhu, X.; Liu, D.; Tang, H.; Luo, G.; Tu, K.; Xie, Z.; Lei, J.; Li, J.; Li, X.; et al. Synthesis of MOF-74-derived carbon/ZnCo<sub>2</sub>O<sub>4</sub> nanoparticles@CNT-nest hybrid material and its application in lithium-ion batteries. *J. Appl. Electrochem.* **2019**, *49*, 1103–1112. [[CrossRef](#)]
14. Bahiraee, Z.; Fathi, S.; Safari, M. Facile synthesis of Fe<sub>3</sub>O<sub>4</sub>@TMU-12 (Co-based magnetic MOF) for extraction of diazinon and chlorpyrifos from the environmental water samples. *Environ. Prog. Sustain.* **2023**, *42*, 1–9. [[CrossRef](#)]
15. Gan, Q.; Zhao, K.; Liu, S.; He, Z. MOF-derived carbon coating on self-supported ZnCo<sub>2</sub>O<sub>4</sub>-ZnO nanorod arrays as high-performance anode for lithium-ion batteries. *J. Mater. Sci.* **2017**, *52*, 7768–7780. [[CrossRef](#)]
16. Chen, J.; Jiang, J.; Liu, S.; Ren, J.; Lou, Y. MOF-derived bimetal oxides NiO/NiCo<sub>2</sub>O<sub>4</sub> with different morphologies as anodes for high-performance lithium-ion battery. *Ionics* **2019**, *25*, 5787–5797. [[CrossRef](#)]
17. Cai, D.; Zhan, H.; Wang, T. MOF-derived porous ZnO/ZnFe<sub>2</sub>O<sub>4</sub> hybrid nanostructures as advanced anode materials for lithium-ion batteries. *Mater. Lett.* **2017**, *197*, 241–244. [[CrossRef](#)]
18. Gao, X.; Du, Y.; Zhou, J.; Li, S.; Qi, P.; Han, Y.; Feng, X.; Jin, X.; Wang, B. Large-scale production of MOF-derived coatings for interlayers in high-performance Li-S batteries. *ACS Appl. Energy Mater.* **2018**, *1*, 6986–6991. [[CrossRef](#)]
19. Li, S.; Yang, H.; Xu, R.; Jiang, Y.; Gong, Y.; Gu, L.; Yu, Y. Selenium embedded in MOF-derived N-doped microporous carbon polyhedrons as a high performance cathode for sodium-selenium batteries. *Mater. Chem. Front.* **2018**, *2*, 1574–1582. [[CrossRef](#)]
20. Koo, W.T.; Jang, H.Y.; Kim, C.; Jung, J.W.; Cheong, J.Y.; Kim, I.D. MOF derived ZnCo<sub>2</sub>O<sub>4</sub> porous hollow spheres functionalized with Ag nanoparticles for a long-cycle and high-capacity lithium ion battery anode. *J. Mater. Chem. A* **2017**, *5*, 22717–22725. [[CrossRef](#)]
21. Suzuki, K.; Mizuno, N.; Yamaguchi, K. Polyoxometalate photocatalysis for liquid-phase selective organic functional group transformations. *ACS Catal.* **2018**, *8*, 10809–10825. [[CrossRef](#)]
22. Gu, J.; Chen, W.; Shan, G.G.; Li, G.; Sun, C.; Wang, X.L.; Su, Z. The roles of polyoxometalates in photocatalytic reduction of carbon dioxide. *Mater. Today Energy* **2021**, *21*, 100760. [[CrossRef](#)]
23. Sun, X.; Zhang, J.; Fu, Z. Polyoxometalate cluster sensitized with copper-viologen framework for efficient degradation of organic dye in ultraviolet, visible, and near-infrared light. *ACS Appl. Mater. Inter.* **2018**, *10*, 35671–35675. [[CrossRef](#)]
24. Zhao, X.; Hang, S.; Yan, J.; Li, L.; Wu, G.; Shi, W.; Yang, G.; Guan, N.; Cheng, P. Polyoxometalate-based metal-organic frameworks as visible-light-induced photocatalysts. *Inorg. Chem.* **2018**, *57*, 5030–5037. [[CrossRef](#)] [[PubMed](#)]
25. Sun, M.; Abazari, R.; Chen, J.; Hussain, C.M.; Zhou, Y.; Kirillov, A.M. Encapsulation of H<sub>4</sub>SiW<sub>12</sub>O<sub>40</sub> into an Amide-Functionalized MOF: A Highly Efficient Nanocomposite Catalyst for Oxidative Desulfurization of Diesel Fuel. *ACS Appl. Mater. Inter.* **2023**, *15*, 52581–52592. [[CrossRef](#)] [[PubMed](#)]
26. Yang, X.; Xie, X.; Li, S.; Zhang, W.; Zhang, X.; Chai, H.; Huang, Y. The POM@MOF hybrid derived hierarchical hollow Mo/Co bimetal oxides nanocages for efficiently activating peroxydisulfate to degrade levofloxacin. *J. Hazard. Mater.* **2021**, *419*, 126360.

27. Mohamed, A.M.; Abbas, W.A.; Khedr, G.E.; Abass, W.; Allam, N.K. Computational and experimental elucidation of the boosted stability and antibacterial activity of ZIF-67 upon optimized encapsulation with polyoxometalates. *Sci. Rep.* **2022**, *12*, 15989. [[CrossRef](#)] [[PubMed](#)]
28. Ammasi, A.; Munusamy, A.P.; Shkir, M.; Maiz, F.; Vellingiri, B.; Minnam Reddy, V.R.; Kim, W.K. Synthesis and electrochemical performance of CoWO<sub>4</sub> and CoWO<sub>4</sub>/MWCNT nanocomposites for highly efficient supercapacitor applications. *Diam. Relat. Mater.* **2023**, *139*, 110352. [[CrossRef](#)]
29. Zeng, T.; Zhang, X.; Wang, S.; Niu, H.; Cai, Y. Spatial confinement of a Co<sub>3</sub>O<sub>4</sub> catalyst in hollow metal-organic frameworks as a nanoreactor for improved degradation of organic pollutants. *Environ. Sci. Technol.* **2015**, *49*, 2350–2357. [[CrossRef](#)] [[PubMed](#)]
30. Liu, B.; Song, W.; Wu, H.; Liu, Z.; Teng, Y.; Sun, Y.; Xu, Y.; Zheng, H. Degradation of norfloxacin with peroxymonosulfate activated by nanoconfinement Co<sub>3</sub>O<sub>4</sub>@ CNT nanocomposite. *Chem. Eng. J.* **2020**, *398*, 125498. [[CrossRef](#)]
31. Ali, J.; Wenli, L.; Shahzad, A.; Ifthikar, J.; Aregay, G.G.; Shahib, I.I.; Elkhilfi, Z.; Chen, Z. Regulating the redox centers of Fe through the enrichment of Mo moiety for persulfate activation: A new strategy to achieve maximum persulfate utilization efficiency. *Water Res.* **2020**, *181*, 115862. [[CrossRef](#)] [[PubMed](#)]
32. Li, J.; Wan, Y.; Li, Y.; Yao, G.; Lai, B. Surface Fe (III)/Fe (II) cycle promoted the degradation of atrazine by peroxymonosulfate activation in the presence of hydroxylamine. *Appl. Catal. B-Environ.* **2019**, *256*, 117782. [[CrossRef](#)]
33. Li, W.; Li, S.; Tang, Y.; Yang, X.; Zhang, W.; Zhang, X.; Chai, H.; Huang, Y. Highly efficient activation of peroxymonosulfate by cobalt sulfide hollow nanospheres for fast ciprofloxacin degradation. *J. Hazard. Mater.* **2020**, *389*, 121856. [[CrossRef](#)]
34. Xue, Y.; Pham, N.N.; Nam, G.; Choi, J.; Ahn, Y.Y.; Lee, H.; Jung, J.; Lee, S.G.; Lee, J. Persulfate activation by ZIF-67-derived cobalt/nitrogen-doped carbon composites: Kinetics and mechanisms dependent on persulfate precursor. *Chem. Eng. J.* **2021**, *408*, 127305. [[CrossRef](#)]
35. Lv, S.W.; Liu, J.M.; Zhao, N.; Li, C.Y.; Yang, F.E.; Wang, Z.H.; Wang, S. MOF-derived CoFe<sub>2</sub>O<sub>4</sub>/Fe<sub>2</sub>O<sub>3</sub> embedded in g-C<sub>3</sub>N<sub>4</sub> as high-efficient Z-scheme photocatalysts for enhanced degradation of emerging organic pollutants in the presence of persulfate. *Sep. Purif. Technol.* **2020**, *253*, 117413. [[CrossRef](#)]
36. Ji, Y.; Dong, C.; Kong, D.; Lu, J. New insights into atrazine degradation by cobalt catalyzed peroxymonosulfate oxidation: Kinetics, reaction products and transformation mechanisms. *J. Hazard. Mater.* **2015**, *285*, 491–500. [[CrossRef](#)]

**Disclaimer/Publisher's Note:** The statements, opinions and data contained in all publications are solely those of the individual author(s) and contributor(s) and not of MDPI and/or the editor(s). MDPI and/or the editor(s) disclaim responsibility for any injury to people or property resulting from any ideas, methods, instructions or products referred to in the content.